Archival Report

Biological Psychiatry

Alterations in Connectome Dynamics in Autism Spectrum Disorder: A Harmonized Mega- and Meta-analysis Study Using the Autism Brain Imaging Data Exchange Dataset

Yapei Xie, Zhilei Xu, Mingrui Xia, Jin Liu, Xiaojing Shou, Zaixu Cui, Xuhong Liao, and Yong He

ABSTRACT

BACKGROUND: Neuroimaging studies have reported functional connectome aberrancies in autism spectrum disorder (ASD). However, the time-varying patterns of connectome topology in individuals with ASD and the connection between these patterns and gene expression profiles remain unknown.

METHODS: To investigate case-control differences in dynamic connectome topology, we conducted mega- and meta-analyses of resting-state functional magnetic resonance imaging data of 939 participants (440 patients with ASD and 499 healthy control subjects, all males) from 18 independent sites, selected from the Autism Brain Imaging Data Exchange (ABIDE) dataset. Functional data were preprocessed and analyzed using harmonized protocols, and brain module dynamics was assessed using a multilayer network model. We further leveraged postmortem brain-wide gene expression data to identify transcriptomic signatures associated with ASD-related alterations in brain dynamics.

RESULTS: Compared with healthy control participants, individuals with ASD exhibited a higher global mean and lower standard deviation of whole-brain module dynamics, indicating an unstable and less regionally differentiated pattern. More specifically, individuals with ASD showed higher module switching, primarily in the medial prefrontal cortex, posterior cingulate gyrus, and angular gyrus, and lower switching in the visual regions. These alterations in brain dynamics were predictive of social impairments in individuals with ASD and were linked with expression profiles of genes primarily involved in the regulation of neurotransmitter transport and secretion as well as with previously identified autism-related genes.

CONCLUSIONS: This study is the first to identify consistent alterations in brain network dynamics in ASD and the transcriptomic signatures related to those alterations, furthering insights into the biological basis behind this disorder.

https://doi.org/10.1016/j.biopsych.2021.12.004

Autism spectrum disorder (ASD) is a highly heritable neurodevelopmental disorder characterized by persistent impairments in social communication and the presence of restricted and repetitive patterns of behavior (1,2). Contemporary views of ASD conceptualize it as a connectome dysfunction syndrome (3,4), manifesting as aberrant functional connectivity in the brain, especially in the default mode network (DMN) (5–8). ASD-related aberrancies in the brain connectome are linked with individual clinical symptoms (8–10) and impairments in cognitive ability (11,12). These studies have provided insights into understanding the biological underpinnings of ASD from a network perspective.

However, despite its importance for understanding the disorder, previous functional connectome studies on ASD have focused primarily on the static (i.e., time-invariant) connectivity patterns, largely ignoring the temporal characteristic of brain networks. The human brain can be thought of as a highly dynamic networked system that exhibits connectivity reconfigurations over time (13,14). These dynamic reconfigurations are essential for efficient intermodule communication (15), flexible cognitive functions (16,17), and rapid response to the external environment (18). Although several prior studies have reported alterations in brain connectome dynamics in ASD, such as increased connectivity variability (19–23) and fewer transitions between connectivity states (24–26), the topological features of dynamic brain networks in ASD remain understudied. Investigating the temporally fluctuating patterns in ASD brain network topology, in particular the properties of modular switching, will advance our understanding of how dynamic interactions of different network components underpin cognitive dysfunction and clinical symptoms in patients (27). Thus, the time-varying pattern of functional connectome topology in ASD is a pertinent area that warrants further research.

Genetic factors are considered to be a predominant cause of ASD (1). Previous twin and family studies have confirmed the

ISSN: 0006-3223

prominent heritability of ASD and ASD-associated traits (28). An increasing number of susceptibility genes have been identified, such as common variants (29) and rare, de novo variants (30). Recently, a large-scale exome sequencing study of ASD identified more than 100 putative ASD-associated risk genes, the majority of which are neuronally expressed (31). RNA microarray and sequencing studies of postmortem ASD brain samples also demonstrated transcriptionally altered genes and affected pathways (32). A recent study suggests that the spatial layout of network module dynamics in healthy brains is linked to the expression level of genes associated with potassium ion channel activity regulation and mitochondria (33). Thus, we speculate that the alteration of brain network dynamics in ASD is related to the expression profile of previously identified autism-related genes.

To address these questions, we conducted the first mega- and meta-analyses for the identification of significant alterations in connectome dynamics in ASD. We used resting-state functional magnetic resonance imaging data from 939 participants selected from 18 independent sites (34,35) and employed a multilayer network model (36) to characterize the topological dynamics of the functional connectome. The mega- and meta-analyses were performed separately, using harmonized image processing and network analysis protocols. Finally, we conducted a partial least squares (PLS) regression analysis to determine the link between abnormal network dynamics and transcriptional profiles. We hypothesized that 1) patients with ASD would show significant alterations in brain connectome dynamics compared with healthy control (HC) subjects, in particular in the DMN regions, and 2) these alterations in brain dynamics would be associated with individual social impairments in patients and the expression profiles of genes that were enriched for previously published ASD-related gene sets.

METHODS AND MATERIALS

Datasets

We selected resting-state functional magnetic resonance imaging data from 440 individuals with ASD and 499 HC subjects (all males; age range, 5–35 years old; collected at 18 independent sites) (Figure S1) from the publicly available Autism Brain Imaging Data Exchange (ABIDE) I and ABIDE II datasets (http://fcon_1000.projects.nitrc.org/indi/abide/) (34,35) after screening based on strict criteria (Supplement).

Data Preprocessing

All resting-state functional magnetic resonance imaging data were preprocessed with a standardized and harmonized pipeline using the GRETNA package (37) (Supplement).

Constructing Dynamic Brain Connectomes

For each individual, dynamic brain connectomes were generated using a sliding window approach (14,38). Specifically, network nodes were defined as 512 regions of interest with uniform areas obtained from a random parcellation (39). Within each time window, we estimated the internode functional connections by calculating the Pearson correlation coefficient between nodal time courses. Here, the window length was set as 60 seconds and the sliding step was set as one repetition time. Finally, we obtained weighted dynamic connectomes by applying a network threshold with a fixed density (density = 15%) to reduce the influence of weak or spurious connectivities (16).

Tracking Dynamic Modular Structures

We used a multilayer network model (36) to identify the time-varying features of connectome topology (Figure 1A). This model incorporates connectivity information from adjacent windows and assumes temporal continuity of modular configurations. Specifically, we conducted a multilayer-variant Louvain algorithm (http://netwiki.amath.unc.edu/GenLouvain) to identify the optimal modular architecture by maximizing the modularity index, Q (range, 0–1), which denotes the extent of segregation between network modules. Then, we computed the modular variability (16) of each brain node to quantify how individual nodes dynamically switched their modular affiliations over time (Supplement). The larger the modular variability, the more flexibly a brain node switches between modules.

Case-Control Comparison Analysis

Mega-analysis. To examine case-control differences in module dynamics, we performed a mega-analysis by pooling individual modular variability maps across all sites. Before performing the analysis, we applied a ComBat harmonization (40–42) to the modular variability maps to correct for site effects. We then estimated group differences in modular variability at both global (whole-brain mean and standard deviation) and nodal levels using a semiparametric generalized additive model (43) with restricted maximum likelihood as the smoothing parameter:

$$\begin{aligned} Y &= \beta_0 + \beta_1 \times \text{group} + f_1(\text{age}) + f_2(\text{age, group}) \\ &\quad + \beta_2 \times \text{mFD} + \varepsilon \end{aligned} \tag{1}$$

where Y denotes the measure of modular variability. The age and age-by-group interaction effects were controlled for by introducing two smooth functions (i.e., f_1, f_2) as nonparametric terms. This allows for flexible assessment of the nonlinear relationship without preemptively assigning a prior shape. Mean framewise displacement (44) was also included as a covariate to control for head motion. Multiple comparisons were corrected for by applying the false discovery rate (FDR) method (45). Cohen's d values, representing the effect size of the group comparisons, were computed from the t-statistic of the group term. The generalized additive model was computed using the mgcv package (https://cran.rproject.org/web/packages/mgcv/index.html). To further decode the cognitive implications of the brain nodes exhibiting ASD-related alterations in connectome dynamics, we performed a functional meta-analysis using the Neurosynth database (46) (Supplement).

Meta-analysis. To assess the robustness of the observed case-control differences in the mega-analysis, we also undertook a harmonized meta-analysis. Briefly, for each site we conducted the generalized additive model (equation 1) to

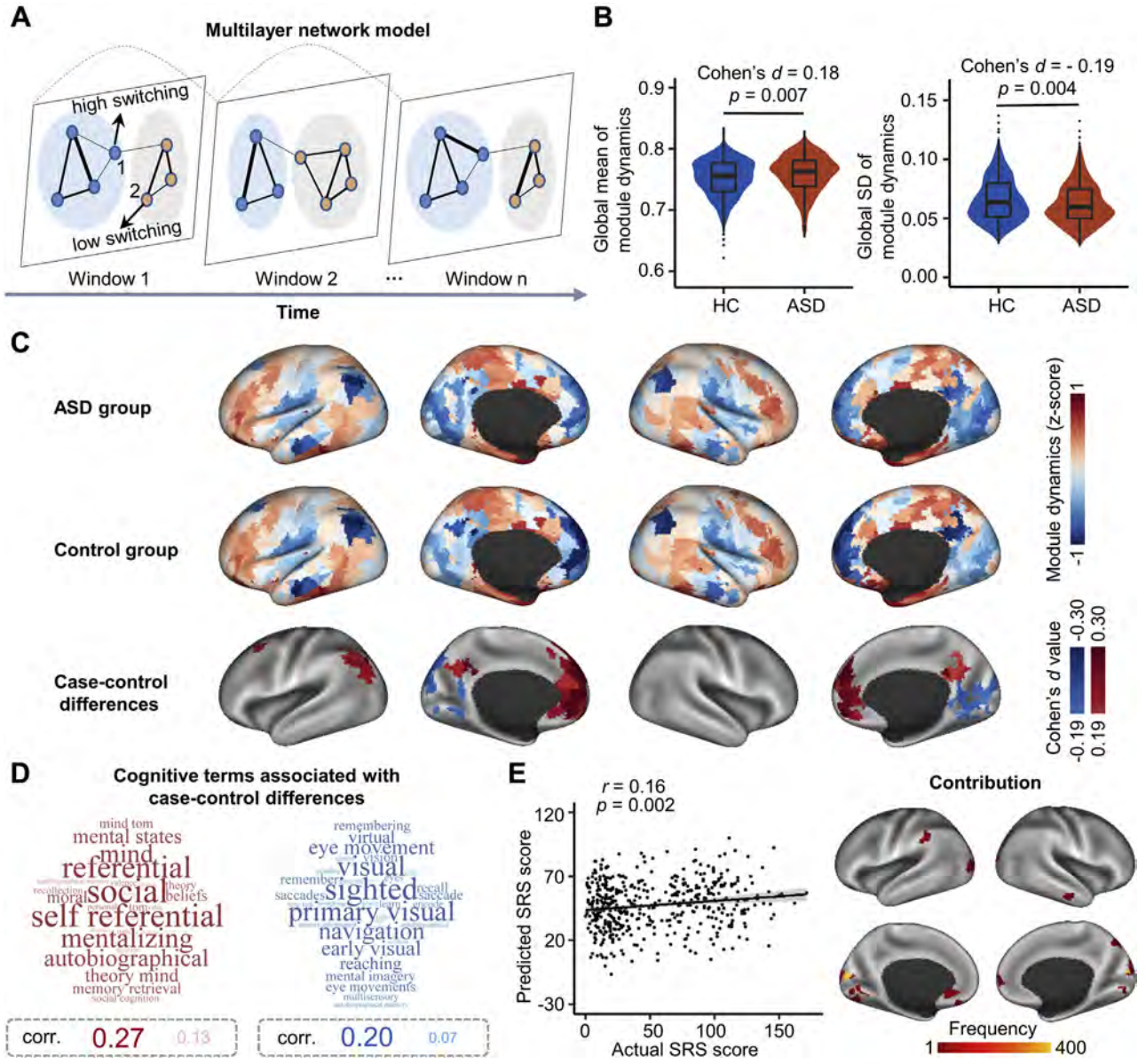

Figure 1. Mega-analysis of case-control differences in module dynamics. **(A)** Schematic overview of brain module switching within a multilayer network model. Each node not only connects to nodes in the same window but also connects to itself in the two temporally adjacent windows. Node colors denote nodal module affiliations. Modular switching is determined by modular variability, which reflects the module dynamics. Node 1 shows a high modular variability, while node 2 shows a low modular variability. **(B)** Mega-analysis of case-control differences in the mean value and the standard deviation of modular variability at the global level. **(C)** Mega-analysis of case-control differences in module dynamics at the nodal level. The upper and middle panels show the group-level modular variability maps for each population. The lower panel shows regions with significant case-control differences in modular variability, corrected for multiple comparisons (false discovery rate–corrected $p < .05$, corresponding to uncorrected $p < .004$). **(D)** Cognitive terms associated with the regions showing significant case-control differences. The red and blue word clouds represent cognitive terms associated with regions showing significantly higher and lower module dynamics, respectively, in the autism spectrum disorder (ASD) group. Font size has been scaled to reflect the correlation value for each cognitive term. **(E)** Prediction of individual Social Responsiveness Scale (SRS) scores based on modular variability maps using support vector regression. The scatterplot displays the correlation between actual and predicted SRS scores. Each dot corresponds to one instance of leave-one-out cross-validation. The brain map displays regional contribution to the prediction, which was defined as the frequency that each region was selected as a feature in the leave-one-out cross-validation. HC, healthy control.

examine site-specific group differences in modular dynamics at both global and nodal levels. Then, we obtained the meta-analytic Cohen's *d* values of these measures using an inverse variance-weighted random effect meta-analysis model in the metafor package (version 3.0.2; https://cran.r-project.org/web/packages/metafor/index.html).

Prediction of Social Impairments Using Connectome Dynamics

We further evaluated whether brain module dynamics were predictive of individual social impairments observed in ASD. To quantify the degree of social impairments, we looked at scores on the Social Responsiveness Scale (SRS), which provides a dimensional characterization of the severity of social impairments related to ASD. We trained a support vector regression model to estimate each participant's SRS score based on the whole-brain modular variability maps. Leave-one-out cross-validation was used to estimate the accuracy of our predictions. In each leave-one-out cross-validation fold, we included the feature selection, model learning, and testing. Nodal contribution to the prediction was defined as the frequency that each node was selected as a feature during the leave-one-out cross-validation (Supplement). This analysis was performed using the LIBSVM toolbox (47).

Association Between Alterations in Connectome Dynamics and Gene Expression Profiles

Estimation of Gene Expression in Brain Nodes. We used the genome expression data from 5 male postmortem human brains from the Allen Human Brain Atlas dataset (48) to identify genes associated with ASD-related alterations in connectome dynamics. Gene expression levels from the left hemisphere were used here, as right hemisphere data were available from only 2 donors. The microarray data were preprocessed using a state-of-the-art analysis pipeline (49) and spatially matched with 222 brain nodes (Supplement). This resulted in a 222 $\times$ 10,145 matrix, denoting the expression of 10,145 genes across 222 nodes.

Spatial Correlation With Gene Expression Profiles. Given the high similarity of results obtained from the mega- and meta-analyses in regard to ASD-related alterations in brain module dynamics (see Results), we performed the connectome-transcriptome association analysis based on the group difference map (i.e., Cohen's *d* values) from the mega-analysis. Specifically, we used a PLS regression to identify the weighted linear combinations (i.e., components) of expression patterns for all 10,145 genes, which were correlated with ASD-related alterations in connectome dynamics. The statistical significance of the variance explained by the PLS components was tested using a permutation analysis (n = 10,000) in which spatial autocorrelation was corrected for (50). For each PLS component map, we calculated the spatial similarity between the weighted gene expressions and Cohen's *d* values in the group difference map using Pearson's correlation. The significance of the correlation was tested again using a permutation analysis (n = 10,000) in which spatial autocorrelation was corrected for (50). Finally, the PLS weight of each gene was transformed into a *z* score value by dividing the weight by the standard deviation of the corresponding weights derived from 1000 instances of bootstrapping (resampling with replacement of 222 nodes). We then ranked all genes according to their z score weights to the PLS components.

Enrichment Analysis. To explore the functional significance of the associated genes, we first conducted separate searches for Gene Ontology terms that were enriched at the top (strong positive correlation) and bottom (strong negative correlation) of the ranked gene list by employing the widely used online tool GOrilla (http://cbl-gorilla.cs.technion.ac.il/) (Supplement) (51). All three ontology classes—biological process, cellular component, and molecular function—were considered.

Next, we performed a gene set enrichment analysis (52) on the whole gene list (i.e., the ordered set of 10,145 genes) to assess whether ASD-related gene sets identified in previous studies were overrepresented in the most strongly correlated genes identified in our ordered list. Specifically, we considered 6 different classes of ASD-related gene sets (Table S1), as follows: gene set 1, ASD-related genes from a summary of multiple datasets (53); gene set 2, ASD risk genes from a large-scale exome sequencing study (31); gene set 3, ASD-associated common genetic variants from a genome-wide association meta-analysis study (29); gene set 4, ASD-associated rare, de novo variants from a study integrating copy number variants and sequencing data (30); gene set 5, genes upregulated in the ASD cortex from a postmortem genome-wide transcriptome study (32); and gene set 6, genes downregulated in the ASD cortex from a postmortem genome-wide transcriptome study (32). For the purposes of comparison, we also included one gene set that was associated with non–mental health diseases (i.e., gene set 7) (53). For each gene set, we obtained an enrichment score representing the level of enrichment. To correct for the size of the gene set, we compared the enrichment score with those estimated from permutation tests (n = 10,000) and derived a normalized enrichment score (NES). The enrichment analysis was performed using the clusterProfiler package version 3.14.3 (https://bioconductor.org/packages/release/bioc/html/clusterProfiler.html) (54).

Power Estimation

We estimated the minimal effect size (i.e., Cohen's *d*) observable for case-control differences between 440 individuals with ASD and 499 HC subjects using G*Power, version 3.1.9.4. At a significant threshold of 0.05 (two-tailed) and a minimum desired power level of 0.8, we had the statistical power to observe Cohen's *d* greater than 0.18.

Validation Analysis

We validated our main findings by considering 8 potential confounding factors, including head motion, window length, multilayer model parameters (i.e., γ and ω), IQ, imaging sites, age range, scanning states, and brain parcellations (Supplement).

RESULTS

Demographic Characteristics

Table 1 summarizes the demographic and clinical information of the participants. No significant difference in age was found between the ASD and HC groups (p = .84). The ASD group showed lower IQ scores ($p = 4.1 \times 10^{-9}$) and higher SRS scores than the HC group ($p = 4.5 \times 10^{-133}$).

Table 1. Demographics and Clinical Characteristics of Participants

	ASD (n = 440)	HC (n = 499)	p Value
Age, Years	5.3–34.5 (14.3 ± 5.4)	5.9–34.1 (14.4 ± 5.4)	.84
FSIQ	71–149 (107.1 ± 16.6)	73–148 (112.8 ± 12.9)	4.1×10^{-9}
ADOS-2 Total (n = 208)	2–26 (11.7 ± 4.2)	NA	
ADOS-2 Severity (n = 208)	1–10 (6.7 ± 2.0)	NA	
ADOS-2 Social (n = 206)	1–20 (8.7 ± 3.6)	NA	
ADOS-2 RRB (n = 209)	0–7 (3.0 ± 1.6)	NA	
ADI-R Social (n = 322)	4–30 (19.3 ± 5.4)	NA	
ADI-R Verbal (n = 322)	4–25 (15.6 ± 4.4)	NA	
ADI-R RRB (n = 322)	0–12 (5.7 ± 2.6)	NA	
SRS: ASD/HC (n = 220/253)	16–171 (90.5 ± 28.7)	0–85 (19.8 ± 13.5)	4.5×10^{-133}

Values are presented as range (mean ± SD). Male participants were selected from 18 of the sites that contributed to the ABIDE I and ABIDE II datasets using stringent quality control criteria. For each clinical measure, we considered only the module/version with the largest sample of participants available. The p value was obtained using a two-sample two-tailed t test.

ABIDE, Autism Brain Imaging Data Exchange; ADI-R, Autism Diagnostic Interview–Revised; ADOS-2, Autism Diagnostic Observation Schedule, Second Edition; ASD, autism spectrum disorder; FSIQ, Full Scale IQ; HC, healthy control; NA, not applicable; RRB, restricted and repetitive behavior; SRS, Social Responsiveness Scale.

Alterations of Module Dynamics in ASD Connectomes

Mega-analysis. At the global level, no significant group difference was found in brain network modularity (p = .32). However, the ASD group showed a higher mean value (Cohen's d = 0.18, p = .007) and a lower standard deviation (Cohen's d = −0.19, p = .004) in whole-brain modular variability than the HC group (Figure 1B). This suggests that global brain dynamics in individuals with ASD tends to be more unstable and regionally undifferentiated compared with that in HC subjects.

At the nodal level, for both the ASD and the HC groups, we observed higher modular variability primarily in the bilateral prefrontal regions and the medial temporal lobe and lower variability mainly in the medial prefrontal and parietal regions, angular gyrus, and visual cortex (Figure 1C, upper and middle panels). This pattern is highly comparable to that shown in previous studies in healthy brains (16,33). Compared with the HC group, the ASD group showed higher modular variability mainly in several DMN regions, including the medial prefrontal cortex, posterior cingulate gyrus, and angular gyrus (Cohen's d range, 0.19–0.33), and lower variability primarily in the visual cortex (Cohen's d range, −0.24 to −0.19) (FDR-corrected $p <$ .05) (Figure 1C, lower panel) (age and age-by-group interaction effects are described in Figure S2 and Figure S3).

Using the NeuroSynth meta-analytic database (46), we found that the regions showing higher modular dynamics in ASD were mainly associated with social function and internally oriented processes, while those showing lower modular dynamics were involved in visual-related tasks (Figure 1D).

Meta-analysis. At the global level, our harmonized meta-analysis revealed that the ASD group showed a higher global mean (Cohen's d = 0.15, p = .01) and a lower standard deviation (Cohen's d = −0.23, p = .001) in whole-brain modular variability compared with the HC group (Figure 2A, B). At the nodal level, the case-control difference pattern was remarkably similar to that derived from the mega-analysis (spatial similarity: r = 0.96, $p <$ .0001 after correcting for spatial autocorrelation) (Figure 2C and Figure S4). The meta-analysis also revealed significant group differences in DMN (Cohen's d range, 0.19–0.34) and visual regions (Cohen's d range, −0.34 to −0.17) (FDR-corrected $p <$ .05) (Figure 2D).

Predicting the Severity of Social Impairments Based on Brain Module Dynamics

Using individual modular dynamics patterns as the feature in the support vector regression model, we found that brain dynamics was a significant predictor of SRS scores (r = 0.16, permutation p = .002) (Figure 1E). Brain nodes making the largest contribution to SRS score prediction were mainly located in the medial prefrontal cortex and the visual cortex (Figure 1E). These regions largely overlapped with regions showing case-control differences in brain modular dynamics.

Association Between Alterations in Connectome Dynamics and Gene Expression Profiles

PLS Regression Analysis. We assessed the spatial association between alterations in ASD-related dynamics and nodal gene expression profiles (Figure 3A). The weighted gene expression pattern of the first PLS component accounted for the greatest spatial variance (20.5%) (Figure 3B) in modular dynamics in the case-control difference map (p = .05, corrected for spatial autocorrelation). The first PLS component score map was spatially correlated with the group difference map (r = 0.45, p = .0043, corrected for spatial autocorrelation) (Figure 3C, D).

Enrichment Analysis. We identified three biological process terms significantly enriched at the top of the gene list: the regulation of secretion by cell, the regulation of neurotransmitter transport, and the regulation of secretion (FDR-corrected $p <$ .01) (Figure 3E). Interestingly, all three of these terms were related to the regulation of transport. We did not find any significant enrichment of Gene Ontology terms at the bottom of the gene list. Moreover, no significant enrichment of molecular function and cellular components was observed.

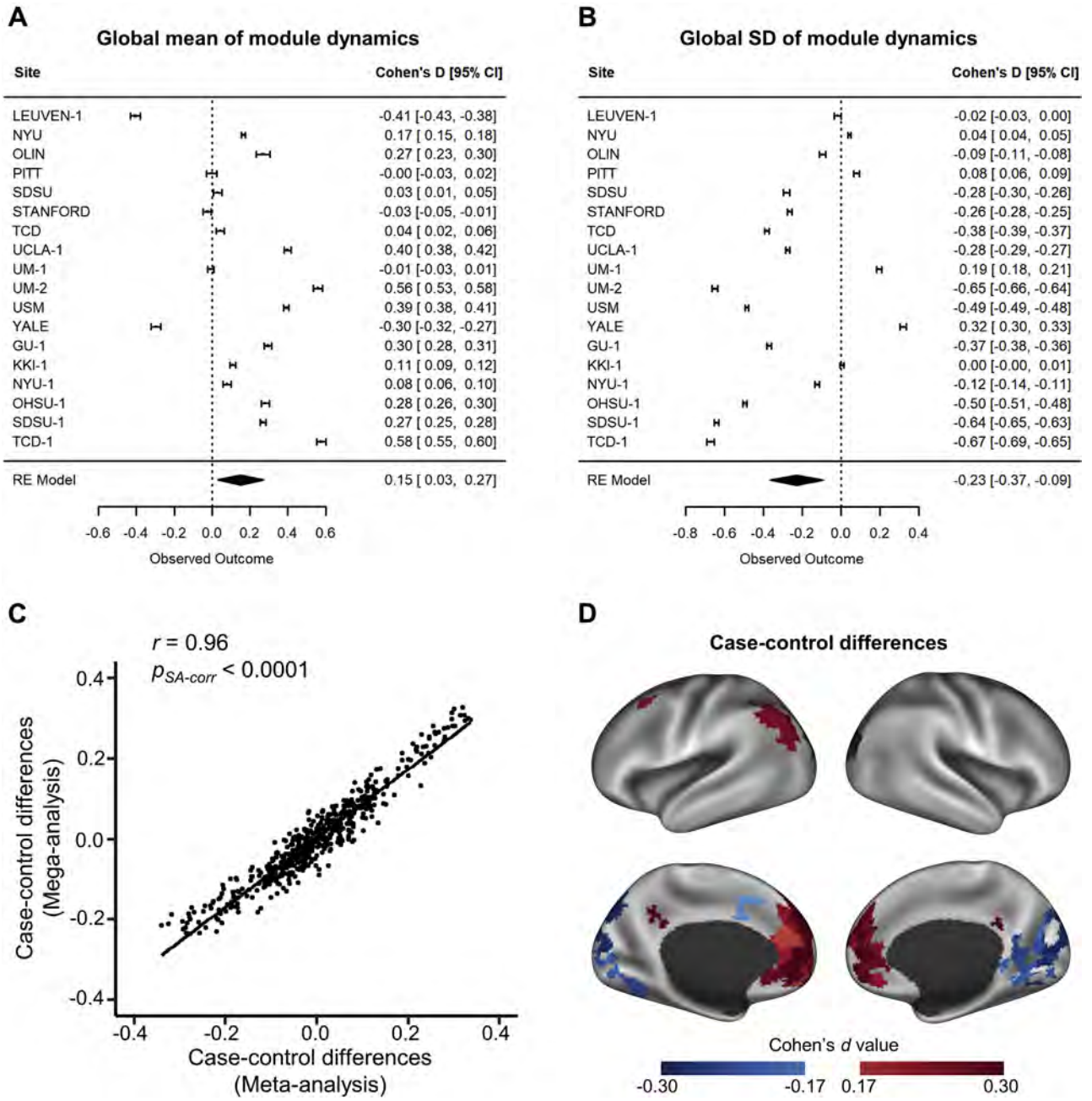

Figure 2. Meta-analysis of case-control differences in module dynamics. **(A)** Forest plot of Cohen's *d* effect sizes for case-control differences in the global mean of modular variability. Each row shows the Cohen's *d* effect size and the confidence intervals for each site. The meta-analysis results are displayed at the bottom with the combined effect and the confidence interval plotted as a diamond. **(B)** Forest plot of Cohen's *d* effect sizes for case-control differences in the standard deviation (SD) of modular variability. **(C)** Spatial similarity between case-control difference maps obtained from the mega- and meta-analyses. Each dot represents a brain node. The significance level of the spatial association was corrected for spatial autocorrelation (SA-corr) (50). **(D)** Meta-analysis of case-control differences at the nodal level. Significance levels of case-control differences in modular variability have been corrected for multiple comparisons (false discovery rate –corrected $p < .05$, corresponding to uncorrected $p < .0056$). Where applicable, samples 1 and 2 are indicated by 1 and 2, respectively, following the site name. GU, Georgetown University; KKI, Kennedy Krieger Institute; LEUVEN, University of Leuven; NYU, NYU Langone Medical Center; OLIN, Olin Institute of Living at Hartford Hospital; PITT, University of Pittsburgh; RE, random effect; SDSU, San Diego State University; STANFORD, Stanford University; TCD, Trinity Center for Health Sciences; UCLA, University of California Los Angeles; UM, University of Michigan; USM, Utah School of Medicine; YALE, Yale School of Medicine.

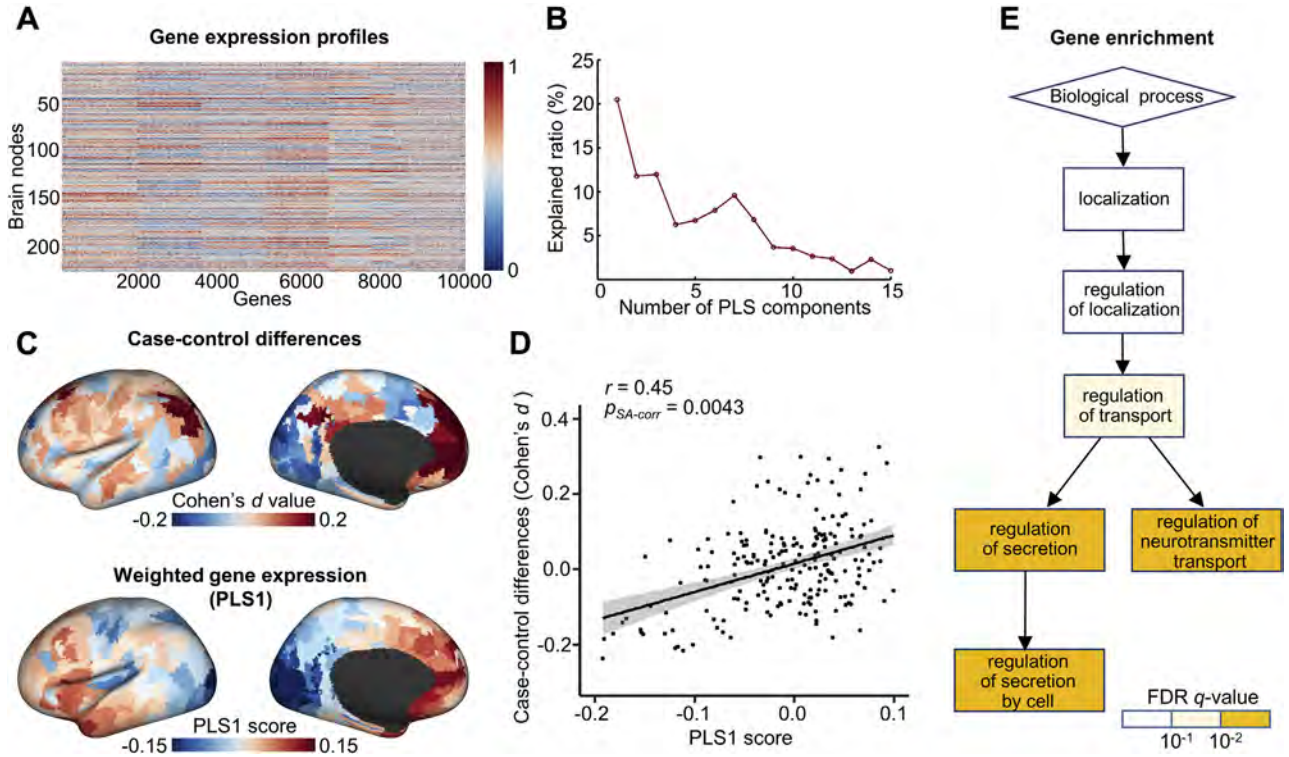

Figure 3. Association between autism spectrum disorder–related alterations in module dynamics and gene expression profiles. **(A)** Gene expression profiles across brain nodes. Each row denotes the gene expression for each gene at a given brain node. **(B)** Explained ratios for the first 15 components obtained from the partial least squares (PLS) regression analysis. Each component denotes a weighted linear combination of the expressions of all genes. **(C)** Spatial patterns showing the mega-analysis case-control differences in modular variability (unthresholded) and the first PLS component (PLS1) scores in the left hemisphere. **(D)** Spatial association between case-control differences in modular variability and PLS1 scores. Each dot represents a brain node. The significance level of the spatial association has been corrected for spatial autocorrelation (SA-corr) (50). **(E)** Significant enrichment of Gene Ontology terms associated with biological processes was observed for top genes with high weights to the PLS1 component. Color denotes the *q* values for the significantly enriched Gene Ontology terms. FDR, false discovery rate.

We further conducted a gene set enrichment analysis to examine whether 6 classes of previously reported ASD-related genes were significantly enriched at the top or bottom of our ordered gene list (Figure 4A). We found that ASD-related genes from a summary of multiple databases (i.e., gene set 1) were significantly enriched at the top of our gene list (NES = 1.27, adjusted p = .035, FDR corrected, hereafter the same) (Figure 4B). The ASD risk genes identified from a large-scale exome sequencing study (i.e., gene set 2) exhibited a significant enrichment at the bottom of our gene list (NES = −1.48, adjusted p = .035) (Figure 4C). We also observed that ASD-related common genetic variants (i.e., gene set 3) were significantly enriched at the bottom of our gene list (NES = −1.70, adjusted p = .028) (Figure 4D), while ASD-related rare, de novo variants (i.e., gene set 4) exhibited only marginally significant enrichment (NES = −1.39, adjusted p = .069) at the bottom of our gene list (Figure 4E). Moreover, genes upregulated and downregulated in postmortem ASD cortex (i.e., gene sets 5 and 6) were significantly enriched at the top and bottom of our gene list, respectively (upregulated: NES = 1.41, adjusted p = .009; downregulated: NES = −1.67, adjusted p = .002) (Figure 4F, G). As a control dataset, the gene set comprising genes associated with non–mental health diseases (i.e., gene set 7) was not significantly enriched at the top or bottom of the gene list (NES = −0.99, adjusted p = .51) (Figure 4H).

Validation Results

When assessing the potential influence of 8 confounding factors, we found that ASD-related, significant alterations in brain modular dynamics remained highly similar to our main results (Table S2; Figures S5 and S6). This suggests that our results were robust and not affected by methodological variations.

DISCUSSION

Using harmonized mega- and meta-analyses, this study provides the first robust demonstration of ASD-related alterations in brain modular dynamics. Our study reveals that these alterations occur primarily in the DMN and visual regions and are associated with social impairments in patients and with the expression profiles of genes enriched for the regulation of neurotransmitter transport and secretion as well as with previously reported autism-related genes. Together, these findings provide evidence for altered macroscopic connectome

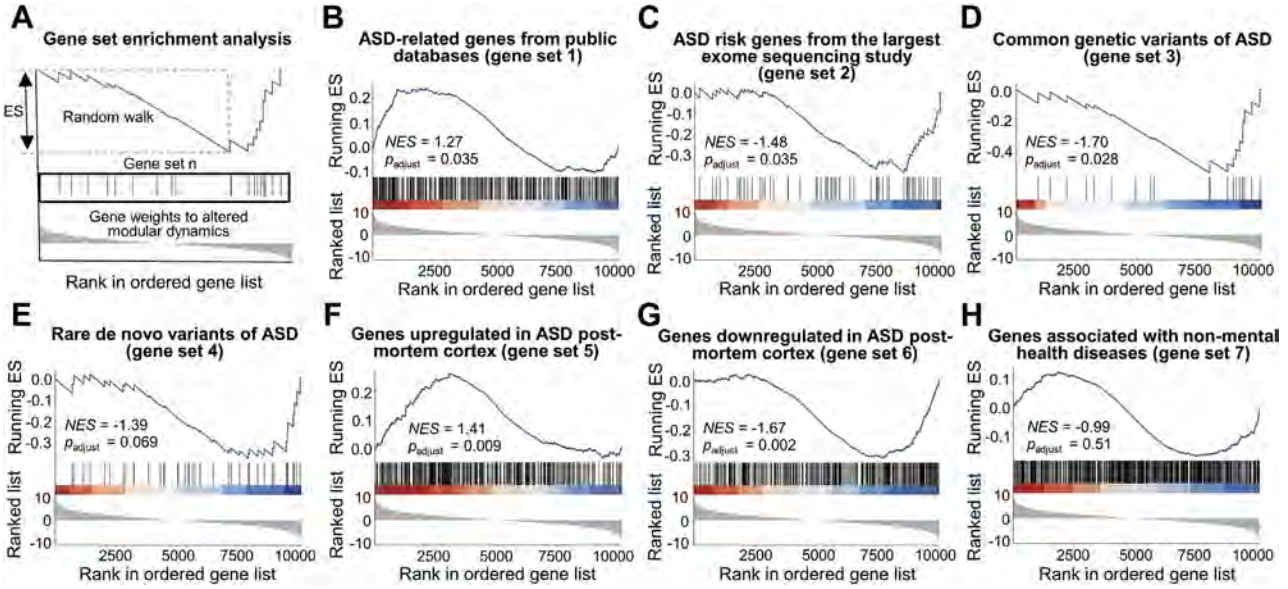

Figure 4. Gene set enrichment analysis of genes associated with autism spectrum disorder (ASD)–related alterations in module dynamics. **(A)** Overview of the gene set enrichment analysis. The solid line denotes the running enrichment score (ES) along the ordered gene list, which increases when a gene is included in the gene set of interest and decreases when a gene is not included. The vertical lines in the middle display the locations at which the members of the gene set appear in the ordered gene list. The shaded curve at the bottom denotes the value of the ranking metric (i.e., *z* value for first partial least squares component weight of each gene) for the genes in the ordered gene list. The ES captures the degree to which the gene set is overrepresented at the top or bottom of the ordered gene list, which is defined as the maximum deviation from zero of the running ES. Significance of the ES was estimated by a gene set–based permutation (10,000 times). **(B)** Significant enrichment of ASD-related genes from a summary of multiple databases (53). **(C)** Significant enrichment of ASD risk genes (31). **(D)** Significant enrichment of common genetic variants of ASD derived from a genome-wide association study (29). **(E)** Marginally significant enrichment of ASD-related rare, de novo variants (30). **(F)** Significant enrichment of genes upregulated in postmortem ASD cortex (32). **(G)** Significant enrichment of genes downregulated in postmortem ASD cortex (32). **(H)** Nonsignificant enrichment of the gene set associated with non–mental health diseases (53). After the gene set enrichment analysis was performed for all gene sets, the ES for each gene set was normalized to the normalized enrichment score (NES) to account for the gene set size, and multiple comparisons with the 7 gene sets were corrected for using the false discovery rate method. p_{adjust}, adjusted *p*.

dynamics and illustrate its linkage with microscopic transcriptional profiles, advancing our knowledge of the biological mechanisms behind ASD.

Aberrant Configuration of Dynamic Modular Architecture in ASD

Existing literature has reported altered static (i.e., time-invariant) functional connectivity in the DMN (5–8) and visual areas (55). Compared with the static-based methods, the connectome dynamics approach used here is able to assess the temporal switching among functional modules. These time-varying features capture regional roles in dynamic inter-module integration (16,56) and the capability of cognitive flexibility (16,17). Specifically, we demonstrated that patients with ASD exhibited higher levels of modular switching in several DMN regions (in particular, the medial prefrontal cortex), but lower modular switching in visual areas, suggesting the aberrance of functional integration between these regions and other network components. Thus, our findings of alterations of ASD-related connectome dynamics provide novel clues into the pathological mechanism behind ASD beyond the static approach.

Based on the meta-analytic Neurosynth decoding, the higher module dynamics in the DMN regions may relate to deficits of cognitive functions, such as self-referential and mentalizing processing (57–59). The lower module dynamics in the visual areas may relate to the dysfunction of visual processing. Prior studies have found that visual perception impairments contribute to early social-emotional deficits (60) and have cascading effects on learning and social development in ASD (61). Thus, we posit that the altered module dynamics underlies impaired social function in individuals with ASD. This speculation was further supported by our analysis predicting individual social impairments using ASD brain dynamics. However, owing to the lack of cognitive data in the ABIDE database, the direct association between the alterations in brain dynamics and the cognition dysfunction warrants further investigation.

Transcriptional Profiling of Aberrant Brain Module Dynamics

Leveraging postmortem brain-wide gene expression data from the Allen Human Brain Atlas dataset (48), we found that ASD-related alterations in brain dynamics were closely associated with the transcriptional profiles of genes involved in the regulation of neurotransmitter transport and secretion. Extensive studies have indicated that aberrant neurotransmitter transport is a significant feature of ASD, especially aberrancies in the transport of the excitatory neurotransmitter glutamate and the inhibitory neurotransmitter GABA (gamma-aminobutyric acid) (62). This suggests that brain regions with abnormal dynamics in ASD, e.g., the medial prefrontal and visual cortices, may have failed to maintain balanced excitatory-inhibitory

neurotransmitter transport. Such speculations are supported by prior studies that have reported imbalanced excitatory-inhibitory synaptic transmission in these regions (63–65). Accordingly, our findings may provide support for the existing excitation/inhibition imbalance theory in ASD (66,67) by revealing a transport regulation–specific connectome-transcriptome association.

We also demonstrated that previously reported autism-related genes were significantly enriched among the genes that we found to be most strongly correlated (both positively and negatively) with alterations in modular dynamics, indicating that different classes of genes contribute to the alterations in module dynamics in ASD. Specifically, compared with rare, de novo variants (gene set 4) (30), ASD-related common genetic variants showed a more substantial influence on module dynamics, which was manifested as a significant enrichment of the gene set. This finding is consistent with a recent study regarding cortical volume and transcriptome association in ASD (68) and could be due to common variants explaining a larger proportion of heritable variance in ASD compared with rare, de novo variants (69). Moreover, we found that genes upregulated and downregulated in postmortem ASD cortex were overrepresented at either the top and bottom, respectively, of our gene list. As the top and bottom weighted genes in the ranked list showed different correlations (i.e., positive and negative) with ASD-related alterations in module dynamics, we speculate that these two categories of dysregulated genes in ASD are likely to affect brain network dynamics in different ways. Several previous studies have also shown the association between abnormal brain morphology (e.g., cortical thickness and volume) and the downregulated genes in ASD, but the same association was not found for the upregulated genes (68,70). Combining these findings, the implication is that different imaging phenotypes in ASD may show common and specific genetic factors. Notably, we did not find any significant overrepresentation of genes in the gene set associated with non–mental health diseases (gene set 7) (53), suggesting that the genes identified as being strongly correlated were specific to mental health disorders.

Limitations and Future Work

First, only male participants were included in this study, given the high prevalence of ASD in males and the small sample of female participants in the ABIDE database. Whether the findings can be generalized to the female population still needs further investigation. Second, we did not exclude individuals with ASD receiving medication, given the limited medication information available from the database. Whether and how medication affects the alterations in module dynamics remains for further exploration. Third, most of our results showed Cohen's *d* effect sizes greater than the power estimation level (i.e., 0.18). Nonetheless, the effect sizes are generally small, which could be due to sample heterogeneity (e.g., ages, subtypes, stages, and medications) and site-related factors (e.g., different scanners and imaging protocols). Fourth, we mainly focused on case-control differences, but age and group-by-age interaction effects were also observed here. As these age and age-by-group interaction effects varied across several validation strategies, these results should be interpreted with caution. Fifth, gene expression data used here were derived from 5 healthy brains. It will therefore be promising to explore the connectome-transcriptome association using ASD gene expression data when the relevant data become available. Finally, as a psychiatric disorder, ASD often features high comorbidity and may exhibit alterations in brain function and genetic factors that are also present in other brain disorders (71,72). Revealing ASD-specific genes and dynamic connectome alterations will be important for understanding the biological basis of this disorder.

ACKNOWLEDGMENTS AND DISCLOSURES

This work was supported by the National Natural Science Foundation of China (Grant Nos. 82021004 [to YH], 81971690 [to XL], 31830034 [to YH], 81620108016 [to YH], 81801779 [to XS], and 11835003 [to XL]), Changjiang Scholar Professorship Award (Grant No. T2015027 [to YH]), Beijing Nova Program (Grant No. Z191100001119023 [to MX]), and Fundamental Research Funds for Central Universities (Grant Nos. 2019NTST24 [to XL] and 2020NTST29 [to MX]).

A previous version of this article was published as a preprint on bioRxiv: https://www.biorxiv.org/content/10.1101/2021.10.03.462909v2.

Participant information and network dynamics data supporting our results are available at https://github.com/helab207/Alterations-in-Connectome-Dynamics-in-ASD-main/tree/main/Data. Codes used for the statistical analysis are available at https://github.com/helab207/Alterations-in-Connectome-Dynamics-in-ASD-main/tree/main/Code.

The authors report no biomedical financial interests or potential conflicts of interest.

ARTICLE INFORMATION

From the State Key Laboratory of Cognitive Neuroscience and Learning (YX, ZX, MX, JL, XS, YH), Beijing Key Laboratory of Brain Imaging and Connectomics (YX, ZX, MX, JL, XS, XL, YH), IDG/McGovern Institute for Brain Research (YX, ZX, MX, JL, XS, YH), and School of Systems Science (XL), Beijing Normal University; and Chinese Institute for Brain Research (ZC, YH), Beijing, China.

Address correspondence to Yong He, Ph.D., at yong.he@bnu.edu.cn, or Xuhong Liao, Ph.D., at liaoxuhong@bnu.edu.cn.

Received Oct 11, 2021; revised Nov 22, 2021; accepted Dec 7, 2021.

Supplementary material cited in this article is available online at https://doi.org/10.1016/j.biopsych.2021.12.004.

REFERENCES

1. Abrahams BS, Geschwind DH (2008): Advances in autism genetics: On the threshold of a new neurobiology. Nat Rev Genet 9:341–355.
2. American Psychiatric Association (2013): Diagnostic and Statistical Manual of Mental Disorders, 5th ed. Arlington, VA: American Psychiatric Publishing.
3. Geschwind DH, Levitt P (2007): Autism spectrum disorders: Developmental disconnection syndromes. Curr Opin Neurobiol 17:103–111.
4. Kana RK, Libero LE, Moore MS (2011): Disrupted cortical connectivity theory as an explanatory model for autism spectrum disorders. Phys Life Rev 8:410–437.
5. Monk CS, Peltier SJ, Wiggins JL, Weng SJ, Carrasco M, Risi S, *et al.* (2009): Abnormalities of intrinsic functional connectivity in autism spectrum disorders. Neuroimage 47:764–772.
6. Lynch CJ, Uddin LQ, Supekar K, Khouzam A, Phillips J, Menon V (2013): Default mode network in childhood autism: Posteromedial cortex heterogeneity and relationship with social deficits. Biol Psychiatry 74:212–219.
7. Assaf M, Jagannathan K, Calhoun VD, Miller L, Stevens MC, Sahl R, *et al.* (2010): Abnormal functional connectivity of default mode subnetworks in autism spectrum disorder patients. Neuroimage 53:247–256.

8. Elton A, Di Martino A, Hazlett HC, Gao W (2016): Neural connectivity evidence for a categorical-dimensional hybrid model of autism spectrum disorder. Biol Psychiatry 80:120–128.
9. Abrams DA, Lynch CJ, Cheng KM, Phillips J, Supekar K, Ryali S, *et al.* (2013): Underconnectivity between voice-selective cortex and reward circuitry in children with autism. Proc Natl Acad Sci U S A 110:12060–12065.
10. Fishman I, Keown CL, Lincoln AJ, Pineda JA, Muller RA (2014): Atypical cross talk between mentalizing and mirror neuron networks in autism spectrum disorder. JAMA Psychiatry 71:751–760.
11. Just MA, Cherkassky VL, Keller TA, Minshew NJ (2004): Cortical activation and synchronization during sentence comprehension in high-functioning autism: Evidence of underconnectivity. Brain 127:1811–1821.
12. Just MA, Cherkassky VL, Keller TA, Kana RK, Minshew NJ (2007): Functional and anatomical cortical underconnectivity in autism: Evidence from an fMRI study of an executive function task and corpus callosum morphometry. Cereb Cortex 17:951–961.
13. Hutchison RM, Womelsdorf T, Allen EA, Bandettini PA, Calhoun VD, Corbetta M, *et al.* (2013): Dynamic functional connectivity: Promise, issues, and interpretations. Neuroimage 80:360–378.
14. Allen EA, Damaraju E, Plis SM, Erhardt EB, Eichele T, Calhoun VD (2014): Tracking whole-brain connectivity dynamics in the resting state. Cereb Cortex 24:663–676.
15. Zalesky A, Fornito A, Cocchi L, Gollo LL, Breakspear M (2014): Time-resolved resting-state brain networks. Proc Natl Acad Sci U S A 111:10341–10346.
16. Liao X, Cao M, Xia M, He Y (2017): Individual differences and time-varying features of modular brain architecture. Neuroimage 152:94–107.
17. Uddin LQ (2021): Brain mechanisms supporting flexible cognition and behavior in adolescents with autism spectrum disorder. Biol Psychiatry 89:172–183.
18. Baker AP, Brookes MJ, Rezek IA, Smith SM, Behrens T, Probert Smith PJ, *et al.* (2014): Fast transient networks in spontaneous human brain activity. Elife 3:e01867.
19. Falahpour M, Thompson WK, Abbott AE, Jahedi A, Mulvey ME, Datko M, *et al.* (2016): Underconnected, but not broken? Dynamic functional connectivity MRI shows underconnectivity in autism is linked to increased intra-individual variability across time. Brain Connect 6:403–414.
20. Chen H, Nomi JS, Uddin LQ, Duan X, Chen H (2017): Intrinsic functional connectivity variance and state-specific under-connectivity in autism. Hum Brain Mapp 38:5740–5755.
21. Li Y, Zhu Y, Nguchu BA, Wang Y, Wang H, Qiu B, *et al.* (2020): Dynamic functional connectivity reveals abnormal variability and hyper-connected pattern in autism spectrum disorder. Autism Res 13: 230–243.
22. Harlalka V, Bapi RS, Vinod PK, Roy D (2019): Atypical flexibility in dynamic functional connectivity quantifies the severity in autism spectrum disorder. Front Hum Neurosci 13:6.
23. Zhang J, Cheng W, Liu Z, Zhang K, Lei X, Yao Y, *et al.* (2016): Neural, electrophysiological and anatomical basis of brain-network variability and its characteristic changes in mental disorders. Brain 139:2307–2321.
24. Fu Z, Tu Y, Di X, Du Y, Sui J, Biswal BB, *et al.* (2019): Transient increased thalamic-sensory connectivity and decreased whole-brain dynamism in autism. Neuroimage 190:191–204.
25. de Lacy N, Doherty D, King BH, Rachakonda S, Calhoun VD (2017): Disruption to control network function correlates with altered dynamic connectivity in the wider autism spectrum. Neuroimage Clin 15:513–524.
26. Watanabe T, Rees G (2017): Brain network dynamics in high-functioning individuals with autism. Nat Commun 8:16048.
27. Khambhati AN, Sizemore AE, Betzel RF, Bassett DS (2018): Modeling and interpreting mesoscale network dynamics. Neuroimage 180:337–349.
28. Ronald A, Hoekstra RA (2011): Autism spectrum disorders and autistic traits: A decade of new twin studies. Am J Med Genet B Neuropsychiatr Genet 156B:255–274.
29. Grove J, Ripke S, Als TD, Mattheisen M, Walters RK, Won H, *et al.* (2019): Identification of common genetic risk variants for autism spectrum disorder. Nat Genet 51:431–444.
30. Sanders SJ, He X, Willsey AJ, Ercan-Sencicek AG, Samocha KE, Cicek AE, *et al.* (2015): Insights into autism spectrum disorder genomic architecture and biology from 71 risk loci. Neuron 87:1215–1233.
31. Satterstrom FK, Kosmicki JA, Wang J, Breen MS, De Rubeis S, An JY, *et al.* (2020): Large-scale exome sequencing study implicates both developmental and functional changes in the neurobiology of autism. Cell 180:568–584.e23.
32. Parikshak NN, Swarup V, Belgard TG, Irimia M, Ramaswami G, Gandal MJ, *et al.* (2016): Genome-wide changes in lncRNA, splicing, and regional gene expression patterns in autism. Nature 540:423–427.
33. Liu J, Xia M, Wang X, Liao X, He Y (2020): The spatial organization of the chronnectome associates with cortical hierarchy and transcriptional profiles in the human brain. Neuroimage 222:117296.
34. Di Martino A, Yan CG, Li Q, Denio E, Castellanos FX, Alaerts K, *et al.* (2014): The autism brain imaging data exchange: Towards a large-scale evaluation of the intrinsic brain architecture in autism. Mol Psychiatry 19:659–667.
35. Di Martino A, O'Connor D, Chen B, Alaerts K, Anderson JS, Assaf M, *et al.* (2017): Enhancing studies of the connectome in autism using the Autism Brain Imaging Data Exchange II. Sci Data 4:170010.
36. Mucha PJ, Richardson T, Macon K, Porter MA, Onnela JP (2010): Community structure in time-dependent, multiscale, and multiplex networks. Science 328:876–878.
37. Wang J, Wang X, Xia M, Liao X, Evans A, He Y (2015): Gretna: A graph theoretical network analysis toolbox for imaging connectomics. Front Hum Neurosci 9:386.
38. Lei T, Liao X, Chen X, Zhao T, Xu Y, Xia M, *et al.* (2021): Progressive stabilization of brain network dynamics during childhood and adolescence [published online ahead of print Aug 10]. Cereb Cortex.
39. Zalesky A, Fornito A, Harding IH, Cocchi L, Yucel M, Pantelis C, *et al.* (2010): Whole-brain anatomical networks: Does the choice of nodes matter? Neuroimage 50:970–983.
40. Fortin JP, Cullen N, Sheline YI, Taylor WD, Aselcioglu I, Cook PA, *et al.* (2018): Harmonization of cortical thickness measurements across scanners and sites. Neuroimage 167:104–120.
41. Yu M, Linn KA, Cook PA, Phillips ML, McInnis M, Fava M, *et al.* (2018): Statistical harmonization corrects site effects in functional connectivity measurements from multi-site fMRI data. Hum Brain Mapp 39:4213–4227.
42. Xia M, Si T, Sun X, Ma Q, Liu B, Wang L, *et al.* (2019): Reproducibility of functional brain alterations in major depressive disorder: Evidence from a multisite resting-state functional MRI study with 1,434 individuals. Neuroimage 189:700–714.
43. Wood SN (2004): Stable and efficient multiple smoothing parameter estimation for generalized additive models. J Am Stat Assoc 99:673–686.
44. Power JD, Barnes KA, Snyder AZ, Schlaggar BL, Petersen SE (2012): Spurious but systematic correlations in functional connectivity MRI networks arise from subject motion. Neuroimage 59:2142–2154.
45. Benjamini Y, Hochberg Y (1995): Controlling the false discovery rate: A practical and powerful approach to multiple testing. J R Stat Soc Series B Stat Methodol 57:289–300.
46. Yarkoni T, Poldrack RA, Nichols TE, Van Essen DC, Wager TD (2011): Large-scale automated synthesis of human functional neuroimaging data. Nat Methods 8:665–670.
47. Chang CC, Lin CJ (2011): Libsvm: A library for support vector machines. ACM Trans Intell Syst Technol 2:1–27.
48. Hawrylycz MJ, Lein ES, Guillozet-Bongaarts AL, Shen EH, Ng L, Miller JA, *et al.* (2012): An anatomically comprehensive atlas of the adult human brain transcriptome. Nature 489:391–399.
49. Arnatkeviciute A, Fulcher BD, Fornito A (2019): A practical guide to linking brain-wide gene expression and neuroimaging data. Neuroimage 189:353–367.

50. Burt JB, Helmer M, Shinn M, Anticevic A, Murray JD (2020): Generative modeling of brain maps with spatial autocorrelation. Neuroimage 220:117038.
51. Eden E, Navon R, Steinfeld I, Lipson D, Yakhini Z (2009): Gorilla: A tool for discovery and visualization of enriched go terms in ranked gene lists. BMC Bioinformatics 10:48.
52. Subramanian A, Tamayo P, Mootha VK, Mukherjee S, Ebert BL, Gillette MA, *et al.* (2005): Gene set enrichment analysis: A knowledge-based approach for interpreting genome-wide expression profiles. Proc Natl Acad Sci U S A 102:15545–15550.
53. Krishnan A, Zhang R, Yao V, Theesfeld CL, Wong AK, Tadych A, *et al.* (2016): Genome-wide prediction and functional characterization of the genetic basis of autism spectrum disorder. Nat Neurosci 19:1454–1462.
54. Yu G, Wang LG, Han Y, He QY (2012): Clusterprofiler: An r package for comparing biological themes among gene clusters. OMICS 16:284–287.
55. Nebel MB, Eloyan A, Nettles CA, Sweeney KL, Ament K, Ward RE, *et al.* (2016): Intrinsic visual-motor synchrony correlates with social deficits in autism. Biol Psychiatry 79:633–641.
56. Pedersen M, Zalesky A, Omidvarnia A, Jackson GD (2018): Multilayer network switching rate predicts brain performance. Proc Natl Acad Sci U S A 115:13376–13381.
57. Lombardo MV, Barnes JL, Wheelwright SJ, Baron-Cohen S (2007): Self-referential cognition and empathy in autism. PLoS One 2:e883.
58. Senju A (2012): Spontaneous theory of mind and its absence in autism spectrum disorders. Neuroscientist 18:108–113.
59. White S, Hill E, Happe F, Frith U (2009): Revisiting the strange stories: Revealing mentalizing impairments in autism. Child Dev 80:1097–1117.
60. Sacrey LA, Armstrong VL, Bryson SE, Zwaigenbaum L (2014): Impairments to visual disengagement in autism spectrum disorder: A review of experimental studies from infancy to adulthood. Neurosci Biobehav Rev 47:559–577.
61. Apicella F, Costanzo V, Purpura G (2020): Are early visual behavior impairments involved in the onset of autism spectrum disorders? Insights for early diagnosis and intervention. Eur J Pediatr 179:225–234.
62. Choudhury PR, Lahiri S, Rajamma U (2012): Glutamate mediated signaling in the pathophysiology of autism spectrum disorders. Pharmacol Biochem Behav 100:841–849.
63. Selimbeyoglu A, Kim CK, Inoue M, Lee SY, Hong ASO, Kauvar I, *et al.* (2017): Modulation of prefrontal cortex excitation/inhibition balance rescues social behavior in cntnap2-deficient mice. Sci Transl Med 9: eaah6733.
64. Sacai H, Sakoori K, Konno K, Nagahama K, Suzuki H, Watanabe T, *et al.* (2020): Autism spectrum disorder-like behavior caused by reduced excitatory synaptic transmission in pyramidal neurons of mouse prefrontal cortex. Nat Commun 11:5140.
65. Robertson CE, Ratai EM, Kanwisher N (2016): Reduced GABAergic action in the autistic brain. Curr Biol 26:80–85.
66. Lee E, Lee J, Kim E (2017): Excitation/inhibition imbalance in animal models of autism spectrum disorders. Biol Psychiatry 81:838–847.
67. Sohal VS, Rubenstein JLR (2019): Excitation-inhibition balance as a framework for investigating mechanisms in neuropsychiatric disorders. Mol Psychiatry 24:1248–1257.
68. Xie Y, Zhang X, Liu F, Qin W, Fu J, Xue K, *et al.* (2020): Brain mRNA expression associated with cortical volume alterations in autism spectrum disorder. Cell Rep 32:108137.
69. Gaugler T, Klei L, Sanders SJ, Bodea CA, Goldberg AP, Lee AB, *et al.* (2014): Most genetic risk for autism resides with common variation. Nat Genet 46:881–885.
70. Romero-Garcia R, Warrier V, Bullmore ET, Baron-Cohen S, Bethlehem RAI (2019): Synaptic and transcriptionally downregulated genes are associated with cortical thickness differences in autism. Mol Psychiatry 24:1053–1064.
71. Morgan SE, Seidlitz J, Whitaker KJ, Romero-Garcia R, Clifton NE, Scarpazza C, *et al.* (2019): Cortical patterning of abnormal morphometric similarity in psychosis is associated with brain expression of schizophrenia-related genes. Proc Natl Acad Sci U S A 116:9604–9609.
72. Sha Z, Wager TD, Mechelli A, He Y (2019): Common dysfunction of large-scale neurocognitive networks across psychiatric disorders. Biol Psychiatry 85:379–388.